Agricultural and Forest Meteorology 304–305 (2021) 108386

Contents lists available at ScienceDirect

Agricultural and Forest Meteorology

journal homepage: www.elsevier.com/locate/agrformet

On the seasonal relation of sun-induced chlorophyll fluorescence and transpiration in a temperate mixed forest

Alexander Damm [a,b,*], Erfan Haghighi [a,b,c], Eugenie Paul-Limoges [a], Christiaan van der Tol [d]

[a] Department of Geography, University of Zurich, Winterthurerstrasse 190, 8057 Zurich, Switzerland
[b] Eawag, Swiss Federal Institute of Aquatic Science and Technology, Überlandstrasse 133, 8600 Dübendorf, Switzerland
[c] Research and Development Department, Oxygen at Work, Kirchgasse 40, 8001 Zurich, Switzerland
[d] University of Twente, Faculty of Geo-Information Science and Earth Observation (ITC), P.O. Box 217, 7500 AE Enschede, the Netherlands

ARTICLE INFO

Keywords:
Stomatal resistance
Abiotic and biotic change driver
Penman-Monteith
Ball-Berry-Leuning
SCOPE
Eddy covariance
Spectroscopy

ABSTRACT

Novel strategies are required to reduce uncertainties in the assessment of ecosystem transpiration (T). A major problem in modelling T is related to the complexity of constraining canopy stomatal resistance (r_{sc}), accounting for the main biological controls on T besides non biological controls such as aerodynamic resistances or energy constraints. The novel Earth observation signal sun-induced chlorophyll fluorescence (SIF) is the most direct measure of plant photosynthesis and offers new pathways to advance estimates of T. The potential of using SIF to study ecosystem T either empirically or in combination with complex mechanistic models has already been demonstrated in recent studies. The diversity of environmental drivers determining diurnal and seasonal dynamics in T and SIF independently requires additional investigation to guide further developments towards robust SIF-informed T retrievals. This study consequently aims to identify relevant biotic and abiotic environmental drivers affecting the capability of SIF to inform estimates of ecosystem T. We used observational data from a temperate mixed forest during the leaf-on period and a Penman-Monteith (PM) based modelling framework, and observed varying sensitivities of SIF-informed approaches for diurnal and seasonal T dynamics (i.e. r^2 from 0.52 to 0.58 and rRMSD from 17 to 19%). We used the PM based modelling framework to investigate systematically the sensitivity of SIF to diurnal and seasonal variations in r_{sc} when empirically and mechanistically embedded in the models. We used observations and the Soil-Vegetation-Atmosphere-Transfer model SCOPE to study the dependence of SIF and T on abiotic and biotic environmental drivers including net radiation, air temperature, relative humidity, wind speed, and leaf area index. We conclude on the potential of SIF to advance estimates of T and suggest preferring more sophisticated modelling frameworks constrained with SIF and other Earth observation data over the single use of SIF to assess reliably ecosystem T across scales.

1. Introduction

Evapotranspiration (ET), the combined flux of water vapor evaporated from soil water and intercepted water on leaf surfaces (E) and transpired through leaf stomata (T), is an important component of the terrestrial water cycle (Jasechko et al., 2013; Wang and Dickinson, 2012). Despite its importance, substantial uncertainties are associated to global estimates of ET. A recent study by Trenberth (2015), for example, indicates that six different Earth system models used to calculate the annual ET flux diverged by up to 37%. Other studies report large uncertainties when partitioning ET between E and T using modelling approaches informed by remote sensing (RS) (Talsma et al., 2018). Current MODIS estimates of average T contributions to ET in vegetated areas range from 20% to 95%, the proportion being highly influenced by the ecosystem type (Schlesinger and Jasechko, 2014). Besides its importance for terrestrial water fluxes, T is key to understanding vegetation-mediated feedbacks between climate and hydrology (Cao et al., 2010; Miralles et al., 2019; Skinner et al., 2018).

Compared to carbon uptake, ecosystem T can be much less constrained with observations and actual estimates are highly uncertain (Coenders-Gerrits et al., 2014; Schlesinger and Jasechko, 2014). Besides sap-flow measurements used to assess T of individual trees (Granier, 1985; Granier, 1987), the eddy covariance (EC) technique enables measurements of ET between vegetated ecosystems and the atmosphere,

* Corresponding author.
E-mail address: adamm@geo.uzh.ch (A. Damm).

https://doi.org/10.1016/j.agrformet.2021.108386
Received 19 May 2020; Received in revised form 25 February 2021; Accepted 26 February 2021
Available online 24 March 2021

e.g. Baldocchi and Ryu (2011). An increasing number of approaches are proposed to partition the measured ET flux into its T and E components (cf. for a review (Jonard, 2020; Kool, 2014; Stoy, 2019) or recent studies (Li et al., 2019; Nelson et al., 2018; Nelson et al., 2020; Perez-Priego et al., 2018; Scanlon and Kustas, 2012; Scott and Biederman, 2017; Zhou et al., 2016)). Overcoming limited spatial representativeness of such in situ measurements is possible with models and RS. Models are typically challenged by the complexity of T. In fact, T is a process controlled by many factors including soil water availability, aerodynamic gradients, available energy, and the biological response to them (i.e. leaf level stomatal conductance (g_s) or the related stomatal resistance (r_{sc})) (Nobel, 2009; Wang and Dickinson, 2012). Particularly r_s at canopy level (r_{sc}), a delicate and dynamic canopy property determined by soil water availability, atmospheric water demand, the release of abscisic acid by the root system, and the photosynthetic carbon demand (Farquhar and Sharkey, 1982), is poorly represented in models and challenging to assess at ecosystem level (Dolman et al., 2014; Franks et al., 2018; Wang and Dickinson, 2012). RS approaches to assess T range from empirical and mechanistic approaches to data assimilation (cf. Wang and Dickinson (2012) for a comprehensive review). Such RS approaches rely on light measurements (i.e. reflected sun radiation and emitted thermal radiation), complemented with several auxiliary data, and only account for potential (rather than actual) photosynthesis (PS) using vegetation greenness. Furthermore, employed observations are representative for process lengths ranging from minutes to years, while instantaneous changes of T are typically not accounted for (Damm et al., 2018).

A new RS approach based on an emitted light signal by plants, sun-induced chlorophyll fluorescence (SIF), has recently been proposed to advance estimates of T (Jonard et al., 2020; Lu et al., 2018; Maes et al., 2020; Qiu et al., 2018; Shan et al., 2021). SIF is the most direct measure of photosynthetic activity (ESA, 2015; Rossini et al., 2015) and its relation to plant carbon assimilation (i.e. gross primary productivity, GPP) has been successfully demonstrated (Damm et al., 2015; Frankenberg et al., 2011; Migliavacca et al., 2017). The accepted theory of a conservative linkage between GPP and T by r_{sc} (Steduto et al., 2007) suggests SIF to possibly advance actual estimates of T. In short, this conservative linkage suggests that the relation of the resistance to diffusion for water and CO_2 is constant for high turbulence, as often the case in field canopies, resulting in a similar impact of r_{sc} on GPP and T (Steduto et al., 2007). Recent studies propose ingesting SIF as a proxy for r_{sc} in mechanistic frameworks (Qiu et al., 2018; Shan et al., 2019; Shan et al., 2021) or to use SIF as a direct surrogate for T (Lu et al., 2018; Maes et al., 2020). The latter implies that SIF is representative for any variable determining T including energy and aerodynamic constrains as well as biological controls on T (i.e. r_{sc}) (cf. Appendix B for a Penman-Monteith (PM) (Monteith, 1965 based modelling of T). Results of these first studies are indeed promising and show an improvement of estimated T at coarser aggregation scales (i.e. average of several days, larger pixel sizes), but Lu et al. (2018) also report a decreasing predictive capability of SIF for instantaneous observations of T. This scaling effect is caused by complex dependencies of the conservative GPP-T relationship on environmental factors (Romero et al., 2004; Singh and Reddy, 2011; Steduto et al., 2007) and a well-known decoupling of PS from g_s for high leaf internal CO_2 (C_i) under specific environmental conditions (i.e. ozone concentrations) (Lombardozzi et al., 2012) and for a range of plant types (Manter and Kerrigan, 2004; Wullschleger, 1993). The mechanistic relation of SIF with the light rather than the dark reaction of PS as well as the insensitivity of SIF for atmospheric constraints (i.e. vapor pressure deficit (VPD)) could additionally explain varying success of purely using SIF when estimating T.

This study consequently aims to demonstrate how key abiotic and biotic drivers compromise the robustness of suggested SIF-informed T approaches that rely on the conservative linkage between GPP and T, under changing environmental conditions at canopy scale. We first employ a PM based modelling framework and differently embed SIF to constrain calculations of T. This stratified approach allows incorporating additional information (e.g. VPD) for T calculations and thus relaxing the demand of SIF being sensitive for all drivers of T dynamics. We then investigate the diurnal and seasonal sensitivity of SIF based r_{sc} estimates with analytically inverted r_{sc} from reference measurements. We use observations of meteorological variables, gas exchange and plant traits in combination with the Soil-Vegetation-Atmosphere-Transfer (SCOPE) model to systematically identify biotic and abiotic environmental drivers possibly confounding SIF-T relationships.

2. Data and methods

2.1. Field observations of T, SIF, and environmental variables

2.1.1. Study site

We used several in situ measurement techniques to acquire an annual cycle of SIF, T and other environmental data needed to constrain aerodynamic, energy, and biological regulations of the PM equation. The forest research site Laegern (47°28′42.0'' N, 8°21′51.8'' E, 682 m a.s.l.) is located on the south-facing slope of a mountain ridge located in the central Swiss Plateau, northwest of the city of Zurich. The mixed temperate forest is composed of a high species diversity, with European beech (*Fagus sylvatica* L.), ash (*Fraxinus excelsior* L.), European silver fir (*Abies alba Mill.*), sycamore maple (*Acer pseudoplatanus*), and Norway spruce (*Picea abies (L.) Karst.*) as the dominant species. The mean tree height of dominant trees is 30.6 m (Etzold et al., 2011). The site has been part of Swiss FluxNet since 2004 and is equipped with an EC flux tower and meteorological measurements. Since 2015, optical measurements are made above the canopy with a UniSpec-DC spectrometer (Paul-Limoges et al., 2018).

2.1.2. Meteorological variables

Environmental variables were measured above the canopy at a height of 47 m including air temperature (T_a) and relative humidity (RH) using a combined temperature and relative humidity probe (Rotronic MP101A, Bassersdorf, Switzerland). Net radiation (R_n) was measured using a CNR 1 four-way net radiometer (Kipp & Zonen B.V., Delft, The Netherlands). Wind speed (U) was measured using a 2D sonic anemometer (WindSonic, Gill Instruments Ltd. Lymington, UK). Measurements were made every 30 s and output averaged every 30 min with a data logger (CR1000, Campbell Scientific Inc., Loughborough, UK) .

2.1.3. Eddy covariance measurement of T and net CO_2 uptake

Continuous turbulent fluxes of CO_2 and water vapor were measured using the EC technique. The EC instrumentation consisted of an open-path infrared gas analyzer (IRGA) (model LI-7500, LI-COR Inc., Lincoln, NE, USA) and a three-dimensional ultrasonic anemometer-thermometer (model HS, Gill Instruments Ltd., Lymington, UK). EC measurements were made at a frequency of 20 Hz. Half-hourly fluxes of CO_2 and water vapor were calculated using the *EddyPro* software (v6.1.0, LI-COR Inc., USA). Frequency response corrections were applied to raw fluxes, accounting for high-pass (Moncrieff et al., 2005) and low-pass filtering (Horst, 1997). Spectral corrections were applied to the fluxes prior to the WPL correction (Webb et al., 1980). Flux quality post-processing was done following Vickers and Mahrt (1997). Standardized gap filling and partitioning of the net ecosystem CO_2 exchange into GPP and ecosystem respiration was performed using the method from Barr et al. (2004). Water vapor fluxes measured with the EC technique represent the combined ET flux. Previous below canopy EC measurements at the site have shown that the below and above canopy fluxes are decoupled under full canopy closure, meaning that under decoupled periods the fluxes measured above canopy represent only the tree canopy (Paul-Limoges et al., 2017). These decoupled periods can be identified using the standard deviation of the vertical wind velocity (σ_w) (Jocher et al., 2017; Paul-Limoges et al., 2017; Thomas et al., 2013). As a result, in order to estimate T from the EC measurements in this study, we

used the ET measurements during (1) decoupled periods (i.e. LAI larger than 3) and (2) excluding times during and the half-hour following rain events greater or equal to 0.1 mm to remove the contribution from intercepted water on leaves. For more details on the T estimates from concurrent below and above canopy EC measurements see Paul-Limoges et al. (2020).

2.1.4. Measurement and retrieval of SIF

A high precision pointing spectrometer (UniSpec-DC, PP Systems International Inc., Amesbury, MA, USA) was installed at the Laegern forest site in January 2015 (Paul-Limoges et al., 2018). The UniSpec-DC samples reflected and emitted radiation in 256 contiguous bands between 350 and 1200 nm with a nominal sampling interval of 3.1 nm. The comparable low spectral resolution was found to compromise the absolute accuracy of SIF retrievals (Damm et al., 2011) but still enables SIF retrievals that are consistent in relative terms (Damm et al., 2011; Zarco-Tejada et al., 2013). Possible biases in absolute accuracy and possible insensitivity for extreme SIF values are, however, not expected to influence the conclusions drawn in this study. The UniSpec-DC simultaneously measures downwelling solar irradiance (I) and upwelling surface reflected radiance (L). The fiber optics from the UniSpec-DC were mounted at 47 m at the Laegern site, pointing south of the tower to avoid any directional influence or shading from the tower. The field of view of the downward fiber optic was 25° and the tilt angle was 10 degrees off nadir. The footprint of the UniSpec-DC was approximately 10 m^2 at the Laegern and included only deciduous trees and not any evergreen trees. Both, upward and downward spectral measurements were taken every 5 minutes and averaged to half-hourly values. SIF at 760 nm (SIF_{760}) was retrieved from the UniSpec radiance measurements around the O_2-A absorption using the three Fraunhofer Line Depth (3FLD) approach as described in (Damm et al., 2014). More details about the method can be found in Appendix-A.

2.2. Forward modelling of T

A key part of this study is to assess robustness of SIF-informed approaches and identify suited strategies to embed SIF in forward modelling T. Therefore, we designed six modelling experiments including three reference experiments without using SIF and three experiments that consider SIF (Table 1). The three reference experiments are based on the PM framework (cf. Appendix-B), while we always used the same set of meteorological variables (i.e. R_n, T_a, RH, U) but differently approximated r_{sc}. In the first implementation, r_{sc} was approximated with a constant LAI (cf. Eq. (S16)). The second implementation approximated r_{sc} as a function of actual LAI (cf. Eq. (S16)). The third approach used the Ball-Berry-Leuning equation (Eq. (S17)), parameterized with meteorological variables and GPP partitioned from EC measurements, to obtain r_{sc} (Eq. (S18)). We then evaluated three strategies to inform T estimates with SIF, while SIF was used with increasing complexity ranging from empirical modelling to mechanistic modelling. The first approach employs a linear empirical relationship between instantaneous observations of SIF with T, while we only adjusted the value range of SIF. The second and third approaches use the PM modelling framework (cf. Appendix-B) fed with meteorological parameters and SIF to i) directly approximate r_{sc} and ii) to approximate A_n in the Ball-Berry-Leuning equation to constrain estimates of g_s (Eq. (S17)) and eventually r_{sc} (Eq. (S18)). We are aware of recent developments (i.e. stomatal optimality models) that challenge the performance of the Ball-Berry-Leuning equation (Ji et al., 2017; Miner et al., 2017; Sperry et al., 2017) but it still provides a robust and established framework. It must be noted that we adjusted the value range of r_{sc} for experiments that explicitly model r_{sc} (i.e. experiment 1-3,5-6) using the value range derived from inverted r_{sc} (cf. Section 2.3)

We note that VPD and r_a are important drivers of T but can be considered as a function of T_a and RH as well as LAI and U, respectively. Since we intend to evaluate the impact of directly measurable parameters on T estimates, we deliberately exclude e.g. VPD and r_a from this specific analysis and do not further disentangle the contribution of

Table 1
Overview of T modelling experiments implemented in this study.

Experiment Nr.	Modelling framework	R_n	T_a	RH	U	r_{sc}
Reference experiments						
1	Penman-Monteith	Measurements				LAI constant
2	Penman-Monteith					LAI actual
3	Penman-Monteith + Ball-Berry-Leuning					Ball-Berry-Leuning: A_n via GPP
SIF experiments						
4	Empirical	SIF				
5	Penman-Monteith	Measurements				SIF
6	Penman-Monteith + Ball-Berry-Leuning					Ball-Berry-Leuning: A_n via SIF

individual observables on e.g. VPD or r_a.

2.3. Inversion of canopy resistance from observations

We used a minimization approach to obtain actual r_{sc} per observation. Therefore, actual EC based T was used as reference, all parameters except r_{sc} were set as measured in situ, and r_s was changed until convergence of measured and modelled T. Convergence was defined as minimum difference (ΔT) between measured T (T_{obs}) and modelled T (T_{sim}) as:

$$\Delta T = |T_{obs} - T_{sim}| \quad (1)$$

It is important to note that resulting r_{sc} is a bulk approximation of r_{sc} but it also absorbs errors stemming from uncertainties in model parameterization and EC based T measurement uncertainty.

2.4. Model based assessment of SIF-T relationships

We performed a simulation experiment to systematically assess the theoretical co-variation of SIF and T with biotic and abiotic environmental drivers. The SCOPE model introduced by van der Tol et al. (2009) allows simultaneous calculations of vegetation spectral radiances (i.e. reflected and emitted fluorescence radiances), as well as gas exchange of ecosystems (i.e. T, A_n) as a function of environmental drivers and plant traits. SCOPE combines a semi-analytical radiative transfer (RT) model based on PROSPECT (Jacquemoud and Baret, 1990) and SAIL (Verhoef and Bach, 2007) to calculate leaf and top-of-canopy (ToC) reflectance and transmittance, an energy balance model providing simulations of gas exchange, photosynthesis, leaf temperature and leaf fluorescence emission, a numerical RT model to calculate ToC emitted thermal radiation (Verhoef et al., 2007) and an RT model for calculating chlorophyll fluorescence at canopy level based on the FluorSAIL model (Miller et al., 2005). The model is a multi-source model where leaf temperature and stomatal resistance are heterogeneous in the canopy, and gas exchange is calculated with the Ball-Berry equation as described in (Collatz et al., 1991).

We set model parameters to best approximate the forest canopy (Table 2). We then varied five model parameters, among them four abiotic drivers (i.e. R_n, T_a, U, RH) and the LAI as the biotic driver in their respective value range (Table 2). Physiological (e.g. the Ball-Berry stomatal conductance parameter (m) representing the Ball-Berry slope parameter a_1 of Eq. (S16), CO_2 compensation point, sensitivity of stomata changes to varying VPD) and leaf meteorological parameters (e.g. leaf surface CO_2 concentration) were kept unchanged since they are hardly accessible at the ecosystem scale. This assumption avoids assessing absolute T values since these parameters change over time, but still allows quantifying the relative impact of R_n, T_a, U, RH, and LAI on T estimates. A_n could not be tested since it is a model output parameter. Soil moisture and other soil properties were assumed constant. Including soil would add another dimension of complexity to related assessments and would require using mechanistic models, e.g. soil-plant-atmosphere continuum (SPAC) models (Garcia-Tejera et al., 2017) that mechanistically connecting soil, plant and atmosphere via water potential gradients (Damm et al., 2018). From the simulations, we extracted far-red SIF at 760 nm and T.

Table 2
Relevant SCOPE model parameters representing a homogeneous forest for the assessment of parameter sensitivities on SIF-T relationships as used in this study.

Parameter	Value
Biochemistry	
Leaf chlorophyll content [μg cm^{-2}]	50
Carotenoid content [μg cm^{-2}]	20
Dry matter content [g cm^{-2}]	0.012
Leaf water content [g cm^{-2}]	0.009
Vcmo [μmol m^{-2} s^{-1}]	60
Ball-Berry stomatal conductance (corresponding to the Ball-Berry slope parameter, cf. Eq. (S16).)	8
Photochemical pathway	C3
Fluorescence quantum yield	0.01
Structure	
Leaf inclination angle parameters []*	-0.35/0.25
Leaf Area Index [m^2 m^{-2}]	1, 2, 4, 6, 8, 10
Canopy height [m]	40
Environment	
Net radiation [W m^{-2}]	100, 300, 500, 700, 900, 1100
Air temperature [°C]	0, 12, 20, 30, 40
Air pressure [hPa]	970
Relative humidity [%] as function of atmospheric vapour pressure [hPa]	4, 25, 45, 66, 87, 99
Wind speed [m]	1, 2, 3, 4, 5, 6

*corresponds to an average leaf zenith angle of 60°.

3. Results

3.1. Dynamics of environmental drivers and plant parameters

We restricted the investigation to a period with canopy closure to enable a reliable estimate of T (Fig. 1). During this time period substantial dynamics in abiotic drivers including R_n (0-600 W m^{-2}), T_a (8-30°C), RH (30-95%) and U (1-4.5m/s) occurred. LAI as the biotic driver ranged between 3 and 6 m^2 m^{-2}, ecosystem functions including GPP (0-45 μmol m^{-2} s^{-1}) and T (0-1 mm h^{-1}) also showed a large range, while SIF varied between 0-1.2 mW m^{-2} sr^{-1} nm^{-1}. Existing dynamics in the available data facilitate assessing relations between SIF and T and investigating the driving force of abiotic and biotic drivers.

3.2. SIF to constrain estimates of T

Six different T modelling approaches were tested, three of them represent the state-of-the-art, and three evaluate the suitability of SIF for T modelling. The standard PM approach with a constant LAI (Fig. 2*A*) revealed a root mean square deviation (RMSD) of 0.14 mm h^{-1} (relative RMSD (rRMSD) of 14%) and an r^2 of 0.66. The use of the actual LAI in PM slightly increased the performance (i.e. r^2 of 0.67, RMSD of 0.14, rRMSD of 14%, Fig. 2*B*), while the combination of PM and the Ball-Berry-Leuning equation parameterized with GPP resulted in a decreased accuracy of modelled T (r^2 of 0.46, RMSD of 0.18, rRMSD of 18%, Fig. 2*C*).

The use of SIF yielded a lower accuracy in modelled T but the accuracy increased with increasing complexity of the modelling framework. The agreement between measured and T modelled as a linear function of SIF (i.e. T=0.86*SIF) was the lowest among the tested approaches with a r^2 of 0.35 and a RMSD of 0.23 mm $hour^{-1}$ (rRMSD of 23.0%) (Fig. 2*D*). The use of SIF in the PM equation yielded an increase in T modelling accuracy (i.e. r^2 of 0.68, RMSD of 0.18, rRMSD of 18%, Fig. 2*E*). The combined use of SIF and coupled PM and Ball-Berry-Leuning equation yielded a moderate accuracy in T modelling compared to the other SIF-based approaches (i.e. r^2 of 0.51, RMSD of 0.20, rRMSD of 20%, Fig. 2*F*).

3.3. Seasonal and diurnal dynamics of canopy resistance

The six approaches tested in the previous section reveal substantial differences, while only the strategy to approximate r_{sc} differed. The assessment of seasonal and diurnal r_{sc} dynamics and corresponding relation of r_{sc} proxies enables further insights in the diversity of T modelling results.

The analytically inverted variation in midday r_{sc} over the vegetation season with closed canopy shows constantly low (around 0 s m^{-1}) but scattered behavior. Only at the beginning (i.e. day 140-150) and end of the period (i.e. day 220-240) midday r_{sc} values tend to slightly increase (Fig. 3, black line in the top panels). It must be noted that the retrieved

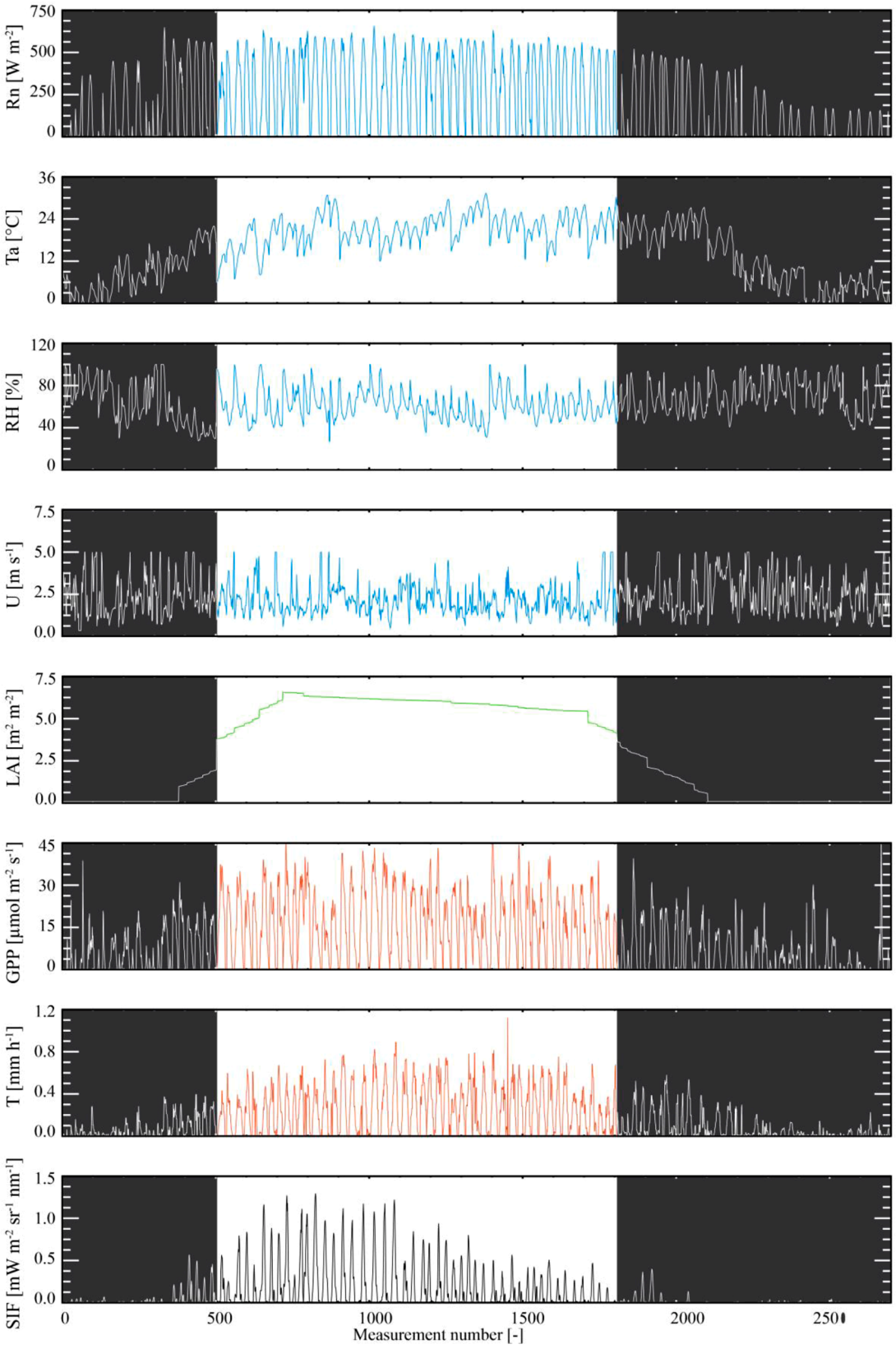

Fig. 1. Dynamics of environmental drivers and plant parameters of the Laegern site, Switzerland. Measurements were obtained in 2016 and correspond to cloud free days with at least 10 valid measurements a day. From top to bottom: Abiotic drivers (blue lines) including net radiation (R_n), air temperature (T_a), relative humidity (RH), wind speed (U); the biotic driver (green line) leaf area index (LAI); functional plant traits (red lines) including net CO_2 uptake (A_n), transpiration (T), and sun-induced chlorophyll fluorescence (SIF). The annual course of LAI was estimated from field observations from 2015 (Paul-Limoges et al., 2017) and cross checked with SIF to exclude errors due to phenological shifts etc. Dates marked in dark grey represent time periods with unclosed canopy cover (LAI<3.0) and were not further analyzed.

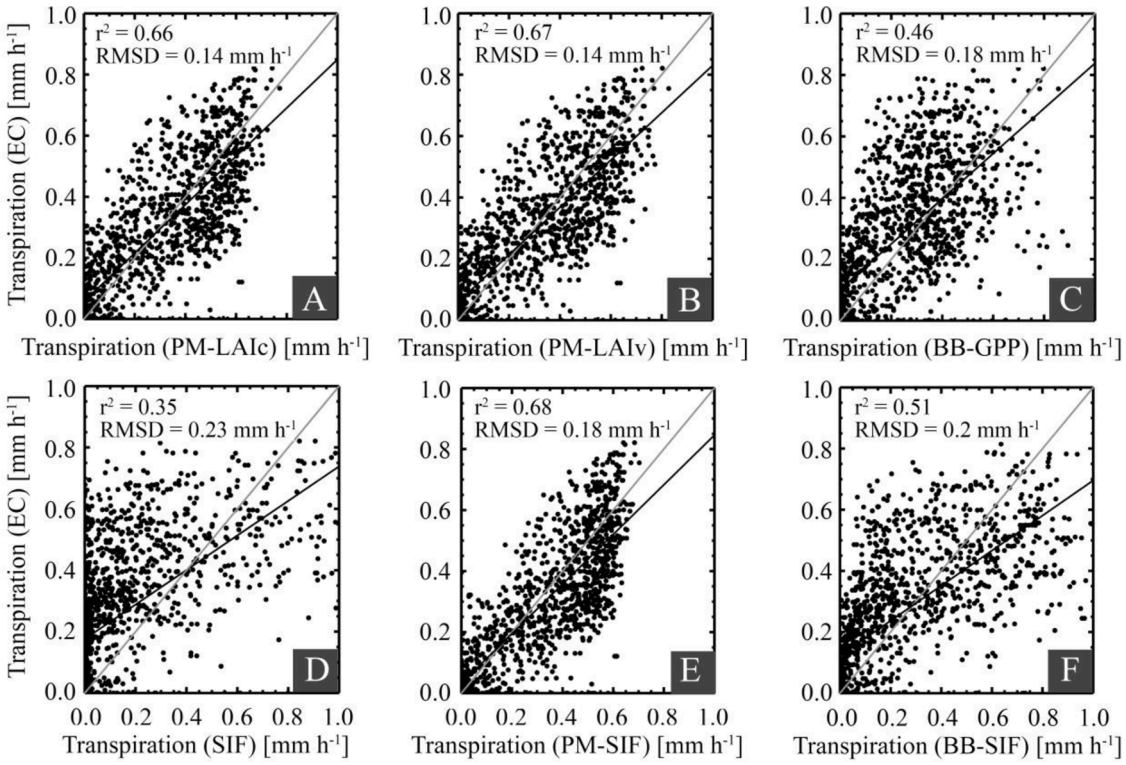

Fig. 2. Correspondence of half-hourly measured and modelled transpiration (T) in a mixed temperate forest over the course of a season with full canopy closure. Only days with cloud-free weather conditions and more than 10 valid measurements are shown. A: T was approximated with the PM equation parameterized with in situ measurements of meteorological variables and a constant LAI as proxy for canopy stomatal resistance (r_{sc}). B: The same as A but with the actual LAI used to approximate r_{sc}. C: r_{sc} was obtained from the Ball-Berry-Leuning equation parameterized with meteorological variables and in situ measured gross primary productivity (GPP). D: T was approximated as linear function of sun-induced chlorophyll fluorescence (SIF). E: The same as A but r_{sc} was approximated with SIF. F: The same as C but SIF was used to approximate A_n in the Ball-Berry-Leuning equation to yield r_{sc}.

r_{sc} value contains sensitivity of real r_{sc}, while a possible bias towards zero values can be explained by inconsistencies of measured ET, PM model input data and model assumption inherent to PM. The use of the actual LAI in PM to approximate r_{sc} results in a rather smooth seasonal dynamic but capturing the slightly increasing r_{sc} values at the beginning and end of the season with an RMSD of 14.2 s m^{-1} and a r^2 of 0.05 (Fig. 3*A*). Using SIF directly to approximate r_{sc} shows a rather insensitive behavior (Fig. 3*B*) with a RMSD of 13.9 s m^{-1} and a r^2 of 0.01. The two approaches that employ GPP and SIF in the Ball-Berry-Leuning equation to retrieve r_{sc} also yield a seasonal r_{sc} signal with slightly higher values beginning and end of season but scatter increases (Fig. 3*C-D*). Corresponding RMSD values range between 45.6 s m^{-1} for the use of GPP in the Ball-Berry-Leuning Equation to 47.6 s m^{-1} when using SIF in the Ball-Berry-Leuning equation.

The assessment of the seasonally averaged diurnal r_{sc} profile shows more pronounced differences across evaluated approaches (Fig. 3, bottom panels). In general, the diurnal profile of retrieved r_{sc} values shows constant decline from the morning to the evening with high values (i.e. above 150 s m^{-1}) in early morning and r_{sc} values around 0 s m^{-1} in the evening. Modelled r_{sc} values mainly show a bowl shaped pattern with highest values in the morning and evening and lowest around noon. It seems that the use of actual LAI can almost recover the analytically retrieved diurnal r_{sc} profile for the morning and afternoon (r^2 = 0.48, RMSD = 37.2 s m^{-1}), while the asymmetric shape (i.e. lower r_{sc} values in the evening) are not fully tracked (Fig. 3*E*). Using the inverse of SIF for $r_{sc} = 1/g_{sc}$ tracks well the diurnal pattern of inverted r_{sc}, while the good behavior in the afternoon can be related to an insensitivity of SIF (flat signal) (r^2 = 0.51, RMSD = 39.0 s m^{-1}) (Fig. 3*F*). Using GPP in combination with the Ball-Berry-Leuning equation (Fig. 3*G*) shows a smooth diurnal pattern with an asymmetry, while the approach substantially underestimates r_{sc} particularly in the morning hours and overestimates in the evening (r^2 = 0.12, RMSD = 69.4 s m^{-1}). Last, using SIF in the Ball-Berry-Leuning equation (Fig. 3*H*) partly captures diurnal dynamics but the signal more noisy and r_{sc} values are substantially overestimated in the afternoon and underestimated in the morning (r^2 = 0.07, RMSD = 55.3 s m^{-1}).

3.4. Impact of environmental drivers on SIF-T relationships

The above assessment indicates that using SIF in process models outperforms the empirical use of SIF to estimate T, but also shows that LAI is better at constraining T than SIF (Fig. 2). This indicates that several confounding factors can disturb the relationship between SIF and T. In fact, T is a complicated process determined by many factors, while SIF is an information source showing a mechanistic relationship to few (i.e. R_n, A_n) but not all essential drivers of T dynamics.

A sensitivity analysis using in situ observations was used to unravel the possible confounding nature of environmental drivers on the SIF-T relationship. Fig. 4 shows corresponding observation of SIF and T, while the data points were colour coded with the value of actual measurements of biotic and abiotic drivers. This analysis enables evaluating when SIF and T are both related due to a possible co-variation with environmental drivers. Fig. 4 indicates that R_n seems to cause a co-variation with T and SIF (i.e. low SIF and T values correspond with low R_n and vice versa), thus couples SIF and T without inherent causality. For other variables, no clear pattern can be observed.

A more sophisticated SCOPE based sensitivity analysis was initiated to complement above investigation with a systematic assessment of environmental driver impact on SIF and T. Fig. 5 shows the varying effect of investigated environmental drivers. While results found for R_n could be confirmed, this systematic analysis also suggests LAI caused large gradients in SIF and T. We could not observe this effect in the

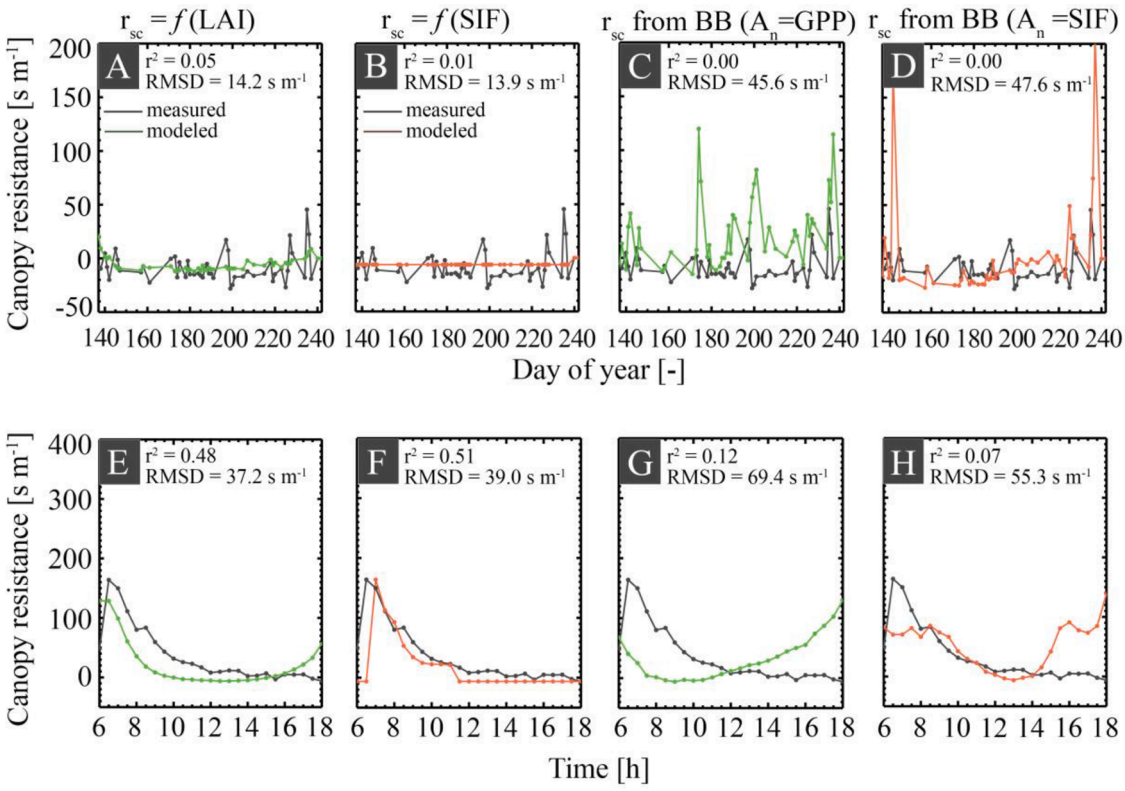

Fig. 3. Dynamics in canopy resistance (r_{sc}) at a seasonal (top panels) and diurnal scale (bottom panels). The black lines correspond to analytically inverted r_{sc} values. Green lines show r_{sc} values obtained from approaches without sun-induced chlorophyll fluorescence (SIF), i.e. using leaf area index (LAI) as direct proxy of r_{sc} (panel A, E) and using gross primary productivity (GPP) in the Ball-Berry-Leuning equation (panel C, G). Red lines show r_{sc} estimated with SIF based approaches i.e. using SIF as direct proxy of r_{sc} (panel B, F) and using SIF in the Ball-Berry-Leuning equation (panel D, H).

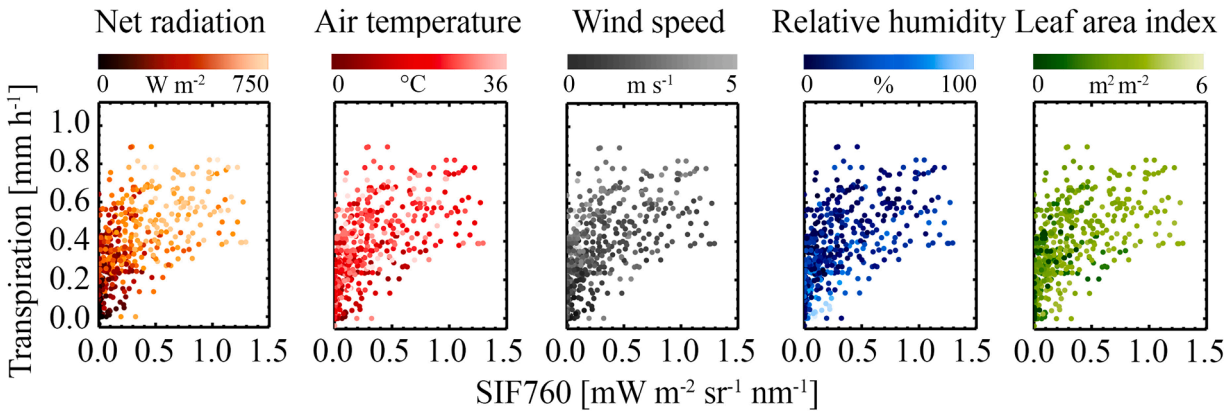

Fig. 4. Correspondence of half-hourly simulated sun-induced chlorophyll fluorescence (SIF) and transpiration (T) for clear sky conditions and full canopy closure (i.e. LAI > 3.0). Measurements represent the Laegern temperate forest in 2016. Corresponding environmental conditions are colour coded with dark and light colours indicating low and high values of the corresponding environmental variables, respectively. A: net radiation (R_n). B: air temperature (T_a). C: wind speed (U). D: relative humidity (RH). E: leaf area index (LAI).

above observational assessment since the value range of LAI during canopy closure was reduced. T_a mainly impacted T but caused substantially less variations in SIF. RH also affected mainly T but to an even smaller extend than T_a. U seemed to have a comparably low impact on SIF and T.

4. Discussion

4.1. Reliability of this analysis

We used a combination of observational data and process modelling to investigate relationships between T and RS measured canopy SIF. Insights revealed from this study are representative for a well-watered mixed temperate forest during canopy closure. The temporal restriction was needed to ensure a reliable approximation of T from ET measurements (cf. Paul-Limoges et al., 2020 for details of the ET partitioning). This certainly reduced the range of naturally existing environmental drivers and their combinations. Further analyses considering different environmental gradients and parameter combinations, different ecosystem types and species, and environmental stresses (e.g. water, temperature, nitrogen) are consequently needed to complement our insights and derive more general conclusions on the

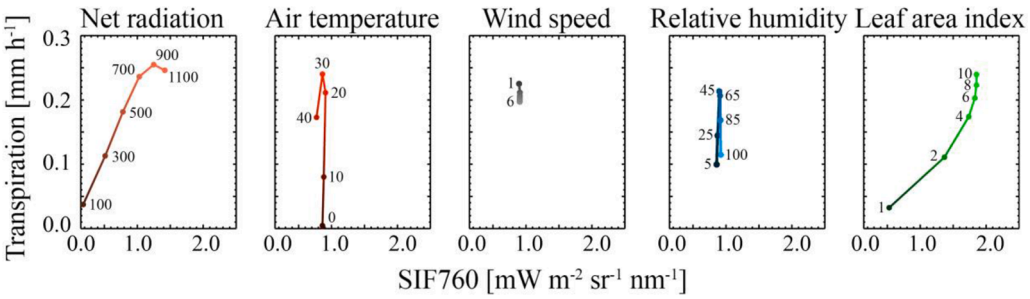

Fig. 5. Modelled relationship between far-red SIF at 760 nm and transpiration for changing environmental drivers obtained from SCOPE. Investigated environmental drivers from left to right: net radiation, air temperature, wind speed, relative humidity, and leaf area index. Dots represent simulated values and lines connect these data points.

impact of environmental drivers on the SIF-T relationship.

Coherence between SIF and T measurements and their sensitivity for T dynamics pose another challenge and asks for a careful interpretation of our results. SIF observations represent mostly the upper canopy layer of a few broadleaved trees. Leaves in such canopy areas often face larger stress during warm and cloud-free days e.g. Williams et al. (1996) compared to leaves in the middle or at the bottom of the canopy. T obtained from EC data, however, represents the vertical integral of all leaves in a larger and changing footprint around the flux tower and includes also evergreen coniferous trees. The diverging footprints are visible in obtained results: Measured A_n and T, for example, indicate a longer phenological cycle compared to SIF that shows a sudden increase in spring and already signs of senescence in summer (cf. Fig. 1). Furthermore, topography related shading causes a decrease of agreement between modelled T using instantaneous SIF compared to measured T (Fig. 3*F*). This is due to a slightly later onset and earlier offset of SIF compared to the full canopy in the flux tower's footprint and caused by topography related lower irradiance received by the observed canopy in the morning and afternoon. The correspondence of RS observations with EC measurements is a factor that needs to be considered and more detailed assessments on the coherence of both observational sources are urgently required to advance mutual evaluation of both information sources (Ryu et al., 2019).

4.2. Mechanistic interrelation between SIF and T

The conceptual reason to use SIF in a T modelling context is founded on the conservative linkage between GPP and T (Steduto et al., 2007) and the sensitivity of SIF for A_n, thus GPP. Several studies, however, indicate that empirical models relating SIF with GPP change across time and ecosystems (Damm et al., 2015; Guanter et al., 2014). This certainly affects the reliability of SIF-based approaches used to model T. Further, SIF is only indirectly linked to A_n while being related to the light reaction of photosynthesis (light harvesting) and not to the dark reaction (carbon fixation). This indirect link is also complicated by dependencies of the SIF-A_n relationship on environmental conditions: Photoprotective mechanisms such as non-photochemical quenching (NPQ) impact SIF-A_n relationships under environmental stress (e.g. excessive light, high temperature, water limitation) (Paul-Limoges et al., 2018; Porcar-Castell et al., 2014). Water stress can additionally determine a variation in observed SIF due to structural changes of leaves since limited water availability can trigger changing leaf angles, causes of shedding leaves, and self-pruning. These aspects explain why there are many attempts to develop approaches that allow compensating for structural effects (Yang et al., 2019; Yang and van der Tol, 2018) and to ingest SIF in modelling frameworks to obtain robust estimates of A_n (ESA, 2015; Fisher et al., 2014; Lee et al., 2015).

T is a highly complex process driven by many environmental drivers and plant properties (Damm et al., 2018; Wang and Dickinson, 2012). The usage of one observable such as SIF to facilitate spatial estimates of T across scales theoretically seems less robust than required (Short Gianotti et al., 2019). Scientifically sound empirical evidence demonstrates, however, seemingly strong relationships between satellite-based SIF measurements and ecosystem T (Lu et al., 2018; Maes et al., 2020). Our study provides insights why such purely SIF based approaches are successful. As shown in Figs. 4 and 5, strong relationships between SIF and T could be partly determined by a co-variance with several environmental drivers over the measurement period. We observe, for example, a strong diurnal and seasonal co-variance of SIF and T with R_n and LAI. For SIF, this finding is in agreement with a modelling study by Verrelst et al. (2015), showing that R_n (or the related APAR) and LAI cause a substantial variation in SIF. Wang and Dickinson (2012), on the other hand, demonstrate R_n, T_a, LAI, soil water availability among the most relevant drivers constraining rates of ecosystem T. Identified co-variance of SIF-T relationships with environmental drivers at coarser aggregation levels does not exclude the possibility of mechanistic relationships between SIF and T. However, our findings strongly suggest that SIF-T relationships are superimposed and partly dominated by a co-variation with R_n and LAI, eventually determining an apparent scale dependency of SIF-T relationships.

4.3. Towards robust SIF-based estimates of T

Increasing evidence suggests that SIF can provide new pathways to assess ecosystem T. Our results indicate that the development of new SIF-based approaches for robust estimates of T across spatial and temporal scales should move beyond the sole use of SIF towards integrated approaches accounting for superimposing environmental factors such as R_n, T_a, or LAI. This conclusion is confirmed by a recent study of Lu et al. (2018), which reports a varying agreement of SIF with T for different spatio-temporal aggregation levels. Also Pagán et al. (2019) found significant but varying relationships between T and SIF across ecosystems. Robust T retrieval strategies should ideally comprise sensitive observations and process modelling (i.e. ranging from simple but robust concepts based on the PM modelling framework (e.g. Shan et al. (2021)) to more complex and driver demanding SPAC or Earth system models). In fact, a recent paper by Qiu et al. (2018), for example, demonstrates that SIF ingested in an Earth system model allows advancing estimates of T (and ET), particularly because it constrains the otherwise not or insufficiently considered biological controls on T (i.e. g_s). Complex mechanistic modelling will also enable better understanding of vertical and horizontal process dynamics and theory development on scaling leaf level processes in complex 3D canopies as recently demonstrated (Damm et al., 2020).

The above suggestion to move towards complex modelling framework implies that reliable information about key environmental drivers are required, particularly R_n, T_a, U, and RH. Other information on vegetation properties (e.g. canopy height, fraction of shaded and illuminated leaves, photosynthetic pathway, root system, canopy roughness), soil properties (e.g. soil water availability, soil poor size), and

environmental variables (e.g. incoming longwave radiation) are also important to model T (Garcia-Tejera et al., 2017; Tuzet et al., 2003) and their impact must be systematically exploited. In this study, we used the PM approach and SCOPE to evaluate the importance of abiotic and biotic driver on SIF-T relationships. Since all models are a simplification of reality, we suggest to extend future analysis with other models and strategies to parameterize system variables (e.g. refer to Su et al. (2001) for a discussion on possibilities and uncertainties to estimate r_a). Further assessments are required to prioritize relevant information prior to generalizing our results for estimating T across scales. The identification of suited missions (e.g. ESA's upcoming FLEX mission) to consistently provide such comprehensive information is also an essential prerequisite to enable reliable cross-scale estimates of T.

5. Conclusions

We conclude that apparent SIF-T relationships are likely caused by a co-variation with few environmental factors, particularly R_n and LAI. This suggests that robustness of T estimates using approaches purely relying on SIF can be compromised temporally and spatially. Our findings are only representative for well-watered mixed temperate forests and complementary analyses in different ecosystem types considering varying environmental stress factors (e.g. water, temperature, nitrogen) are essential to further assess sensitivity limits of SIF for T estimates.

We suggest incorporating SIF into more complex modelling frameworks (e.g. PM, SPAC) to account for possible co-variance of environmental drivers with both SIF and T, to consider mechanisms of underlying processes and eventually to increase robustness of SIF-based T estimates across scales. In addition, emphasis should be on evaluating and possibly improving retrievals of other critical environmental drivers from RS data as identified in this study (particularly R_n, T_a and RH) and factors not directly accessible by RS but known to be of importance (e.g. soil moisture, root properties) to allow cross-scale estimates of T.

SIF is the most direct RS observation of ecosystem photosynthesis and offers new avenues to assess gas exchange between plants and the atmosphere at the ecosystem scale. Both carbon exchange and T are determined by stomatal resistance and the development of novel SIF-based T assessment schemes will cause mutual benefits to stimulate both carbon and water cycle research besides contributing to a decrease of the current 37% uncertainty in global ET flux estimates.

Declaration of Competing Interest

The authors declare that they have no known competing financial interests or personal relationships that could have appeared to influence the work reported in this paper.

Acknowledgements

E.H. acknowledges funding from the Swiss Federal Institute of Aquatic Science and Technology (Eawag). This study used eddy covariance and meteorological data acquired in frame of the Swiss FluxNet initiative and we are grateful to the Grasland Science Group at ETH Zurich for generating this high quality data. We are grateful to the two anonymous reviewers for providing excellent and highly constructive comments to improve this manuscript.

Appendix A. Retrieval of sun-induced chlorophyll fluorescence

SIF at 760 nm (SIF_{760}) was retrieved from the UniSpec radiance measurements around the O_2-A absorption using the three Fraunhofer Line Depth (3FLD) approach as described in Damm et al. (2014). The method, in short, employs two radiance measurements L_i inside (i, 760 nm) and L_o outside (o) of the O_2-A band to decouple fluorescence from the reflected radiance. A radiance measurement can be expressed as:

$$L_j = L_j^p + \frac{\left(I_j^g \frac{\rho_j}{\pi} + SIF_j\right)\tau\uparrow_j}{1 - S_j * \rho_j},\ j = \{i, o\}, \tag{S1}$$

L^p is the path scattered radiance, I^g is the global irradiance (including direct and diffuse irradiance components) arriving on the surface, ρ is the surface reflectance, $\tau\uparrow$ is the upwelling transmittance, and S is the spherical albedo. I^g was directly measured with the upward looking channel. We assumed $L^p = 0$ and $\tau\uparrow = 1$, justified by the short distance between surface and sensor (< 10 m). Further, S was set to zero since the product of S and ρ can be assumed as << 1. The remaining four unknown variables of the system of equations (Eq. (S1)) (i.e. ρ_i, ρ_o, SIF_i, SIF_o) had to be reduced to only two to eventually retrieve SIF. We applied the 3FLD approach originally introduced by Maier et al. (2003) to linearly relate ρ and SIF inside and outside of the O_2-A band. With this, SIF_{760} can be retrieved as:

$$SIF_{760} = SIF_i = B\left[\frac{X_i\left(I_o^* + X_o \cdot S_o\right) - AX_o\left(I_i^* + X_i \cdot S_i\right)}{B\left(I_o^* + X_o \cdot S_o\right) - A\left(I_i^* + X_i \cdot S_i\right)}\right],\ \text{with} \tag{S2}$$

$$X_j = \frac{\left(L_j - L_j^p\right)}{\tau\uparrow_j},\ I_j^* = \frac{I_j^g}{\pi},\ j = \{i, o\},\ \text{and} \tag{S3}$$

$$\left.\begin{array}{l}\rho_i = A\rho_o \\ F_i = BF_o\end{array}\right\} \tag{S4}$$

X_j equals the top-of-canopy (ToC) radiance leaving the surface. A is the factor relating ρ_i, and ρ_o and was derived from linear interpolation of ρ_o using the left (average 730-745 nm) and right (average of 764-780 nm) O_2-A band shoulders with:

$$A = \frac{\rho_{737}\omega_1 + \rho_{772}\omega_2}{\rho_{737}}, \tag{S5}$$

$$\omega_1 = \frac{772 - 760}{772 - 737},\ \text{and}\ \omega_2 = \frac{760 - 737}{772 - 737}. \tag{S6}$$

B is a factor relating F inside and outside the O_2-A band and was fixed to a value of 1.0, justified by simulations and experiments.

Appendix B. Penman-Monteith based modelling framework

The PM equation (Monteith, 1965) in combination with a well-established representation of g_s introduced by Ball, Berry, and Leuning (Ball et al., 1987; Leuning, 1990; Leuning, 1995) provides an efficient framework to ingest RS data for T estimation. The PM equation follows a single-layer or "big leaf" approach and enables estimating T as:

$$T = \frac{\Delta(R_n - G) + p_a c_p \frac{VPD}{r_a}}{\Delta + \gamma\left(1 + \frac{r_{sc}}{r_a}\right)} \tag{S7}$$

where R_n is the net radiation, G is the ground heat flux, p_a is the density of dry air, c_p is the specific heat capacity of air, VPD is the vapor pressure deficit, r_a is the aerodynamic resistance, Δ is the slope of saturated vapor pressure curve with air temperature, γ is the psychometric constant, and r_{sc} is a bulk stomatal resistance describing the resistance to flow of water vapor from inside the big leaf surface (or vegetation canopy) to outside the surface.

Except for r_{sc}, all these variables can be either directly measured (R_n) or expressed as a function of a few measurable meteorological variables (i.e. air temperature (T_a), wind speed (U) and relative humidity (RH)), surface height (z) and physical constants.

Following Tetens (1930) and Murray (1967), Δ can be calculated as:

$$\Delta = \frac{4098\left[0.6108\ \exp\left(\frac{17.72T_a}{T_a+273.3}\right)\right]}{(T_a + 273.3)^2} \tag{S8}$$

and γ can be obtained from:

$$\gamma = 0.000665p \tag{S9}$$

where surface pressure (p) is a function of z and can be approximated as:

$$p = 101.3\left(\frac{293 - 0.0065z)}{293}\right)^{5.26} \tag{S10}$$

Specific heat capacity c_p can be calculated as:

$$c_p = \frac{\gamma e l}{p} \tag{S11}$$

where l is the latent heat of vaporization (2.45 MJ kg^{-1}) and e is the ratio of the molecular weight of water vapor and dry air (i.e. 0.622).

Still following Tetens (1930) and Murray (1967), p_a can be calculated as:

$$p_a = \frac{p}{1.01(T_a + 273)R} \tag{S12}$$

where R is the specific gas constant of 0.287 kJ kg^{-1} K^{-1}.

VPD is defined as the difference between saturation vapour pressure (e_s) and actual vapour pressure (e_a):

$$e_s = 0.6108\exp\left[\frac{17.72T_a}{T_a + 237.3}\right] \tag{S13}$$

$$e_a = e_s\frac{RH}{100} \tag{S14}$$

r_a can be finally approximated according to Allen et al. (1998) as:

$$r_a = \frac{\ln\left[\frac{z_m - d}{z_{om}}\right]\ln\left[\frac{z_h - d}{z_{oh}}\right]}{k^2 u_z^*} \tag{S15}$$

where, z_m is the height of wind measurements, z_h is the height of humidity measurements, d is the zero plane displacement height, z_{om} is the roughness length for momentum transfer, z_h is the roughness length for heat and vapor transfer, and k=0.41 is the von Kármán constant.

The biological control is embedded in r_{sc}, representing g_s integrated over all leaves of the canopy, the canopy conductance (g_{sc}). g_s is directly or indirectly related to varying environmental drivers such as soil water availability, possible discharge of abscisic acid for certain species under water stress, water potential gradients between leaf internal and exterior, leaf internal CO_2 concentration and actual photosynthetic rates, etc.

In the standard PM approach, canopy level r_{sc} can be directly approximated as function of LAI and an approximation of a bulk leaf level stomatal resistance (r_s) of a well illuminated leaf as

$$r_{sc} = \frac{r_s}{0.5\ LAI} \tag{S16}$$

The Ball-Berry-Leuning model allows expressing g_s, i.e. the inverse of r_s, as (Ball et al., 1987; Leuning, 1990; Leuning, 1995):

$$\frac{1}{r_s} = g_s = g + \frac{a_1 A_n}{(C_s - \Gamma)\left(1 + \frac{VPD}{D_O}\right)} \quad \text{(S17)}$$

where g_s is the stomatal conductance for CO_2 diffusion, a_1 and g are empirical factors describing slope and minimum conductance, A_n is the actual net photosynthetic rate, C_s is the leaf-surface CO_2 concentration, and Γ is the CO_2 compensation point, and D_o is an empirical parameter representing the sensitivity of stomata changes to VPD. In our implementation, we used alternatively measured gross primary productivity (GPP) and SIF as direct proxy of A_n in Eq. (S17).

Although g_s of shaded and illuminated leaves substantially varies, g_{sc} and r_{sc} is often derived by multiplying g_s with the leaf area index (LAI) assuming that all leaves equally contribute to g_{sc} (Ding et al., 2014):

$$r_{sc} = \frac{1}{g_s} LAI \quad \text{(S18)}$$

Supplementary materials

Supplementary material associated with this article can be found, in the online version, at doi:10.1016/j.agrformet.2021.108386.

References

Allen, R.G., Pereira, L.S., Raes, D., Smith, M., 1998. Crop Evapotranspiration - Guidelines for Computing Crop Water Requirements. FAO Irrigation and Drainage Paper 56. Food ans Agricultural Organization, Rome.

Baldocchi, D.D., Ryu, Y., 2011. A synthesis of forest evaporation fluxes - from days to years - as measured with eddy covariance. Ecol. Stud. - Anal. Synth. 216, 101–116.

Ball, J.T., Woodrow, I.E., Berry, J.A., 1987. A model predicting stomatal conductance and its contribution to the control of photosynthesis under different environmental conditions. Progress in Photosynthesis Research. Springer Netherlands, pp. 221–224.

Barr, A.G., et al., 2004. Inter-annual variability in the leaf area index of a boreal aspen-hazelnut forest in relation to net ecosystem production. Agric. For. Meteorol. 126 (3-4), 237–255.

Cao, L., Bala, G., Caldeira, K., Nemani, R., Ban-Weiss, G., 2010. Importance of carbon dioxide physiological forcing to future climate change. PNAS 107 (21), 9513–9518.

Coenders-Gerrits, A.M.J., et al., 2014. Uncertainties in transpiration estimates. Nature 506 (7487), E1–E2.

Collatz, G.J., Ball, J.T., Grivet, C., Berry, J.A., 1991. Physiological and environmental-regulation of stomatal conductance, photosynthesis and transpiration - a model that includes a laminar boundary-layer. Agric. For. Meteorol. 54 (2-4), 107–136.

Damm, A., et al., 2011. Modeling the impact of spectral sensor configurations on the FLD retrieval accuracy of sun-induced chlorophyll fluorescence. Remote Sens. Environ. 115 (8), 1882–1892.

Damm, A., et al., 2014. FLD-based retrieval of sun-induced chlorophyll fluorescence from medium spectral resolution airborne spectroscopy data. Remote Sens. Environ. 147, 256–266.

Damm, A., et al., 2015. Far-red sun-induced chlorophyll fluorescence shows ecosystem-specific relationships to gross primary production: an assessment based on observational and modeling approaches. Remote Sens. Environ. 166, 91–105.

Damm, A., et al., 2018. Remote Sensing of plant-water relations: an overview and future perspectives. J. Plant Physiol. 277, 3–19.

Damm, A., Paul-Limoges, E., Kückenbrink, D., Bachofen, C., Morsdorf, F., 2020. Remote sensing of forest gas exchange: considerations derived from a tomographic perspective. Glob. Change Biol. 26 (4), 2717–2727.

Ding, R.S., Kang, S.Z., Du, T.S., Hao, X.M., Zhang, Y.Q., 2014. Scaling up stomatal conductance from leaf to canopy using a dual-leaf model for estimating crop evapotranspiration. PLoS One 9 (4).

Dolman, A.J., Miralles, D.G., de Jeu, R.A.M., 2014. Fifty years since Monteith's 1965 seminal paper: the emergence of global ecohydrology. Ecohydrology 7 (3), 897–902.

ESA, 2015. Report for Mission Selection: FLEX. ESA SP-1330/2 (2 volume series). European Space Agency, Noordwijk, The Netherlands.

Etzold, S., et al., 2011. The carbon balance of two contrasting mountain forest ecosystems in Switzerland: similar annual trends, but seasonal differences. Ecosystems 14 (8), 1289–1309.

Farquhar, G.D., Sharkey, T.D., 1982. Stomatal conductance and photosynthesis. Annu. Rev. Plant Physiol. Plant Mol. Biol. 33, 317–345.

Fisher, J.B., Huntzinger, D.N., Schwalm, C.R., Sitch, S., 2014. Modeling the terrestrial biosphere. Annu. Rev. Environ. Resour. 91–123.

Frankenberg, C., et al., 2011. New global observations of the terrestrial carbon cycle from GOSAT: Patterns of plant fluorescence with gross primary productivity. Geophys. Res. Lett. 38.

Franks, P.J., et al., 2018. Comparing optimal and empirical stomatal conductance models for application in Earth system models. Global Change Biol. 24 (12), 5708–5723.

Garcia-Tejera, O., Lopez-Bernal, A., Testi, L., Villalobos, F.J., 2017. A soil-plant-atmosphere continuum (SPAC) model for simulating tree transpiration with a soil multi-compartment solution. Plant Soil 412 (1-2), 215–233.

Granier, A., 1985. Une nouvelle méthode pour la mesure du flux de sève brute dans le tronc des arbres. Ann. For. Sci. 42 (2), 193–200.

Granier, A., 1987. Evaluation of transpiration in a Douglas-fir stand by means of sap flow measurements. Tree Physiol. 3 (4), 309–320.

Guanter, L., et al., 2014. Global and time-resolved monitoring of crop photosynthesis with chlorophyll fluorescence. PNAS 111 (14), E1327–E1333.

Horst, T.W., 1997. A simple formula for attenuation of eddy fluxes measured with first-order-response scalar sensors. Bound. Layer Meteorol. 82 (2), 219–233.

Jacquemoud, S., Baret, F., 1990. Prospect - a model of leaf optical-properties spectra. Remote Sens. Environ. 34 (2), 75–91.

Jasechko, S., et al., 2013. Terrestrial water fluxes dominated by transpiration. Nature 496 (7445), 347–350.

Ji, S., et al., 2017. A modified optimal stomatal conductance model under water-stressed condition. Int. J. Plant Prod. 11 (2), 295–314.

Jocher, G., et al., 2017. Apparent winter CO2 uptake by a boreal forest due to decoupling. Agric. For. Meteorol. 232, 23–34.

Jonard, F., et al., 2020. Value of sun-induced chlorophyll fluorescence for quantifying hydrologicalstates and fluxes: current status and challenges. Agric. For. Meteorol. 291, 108088.

Kool, D., et al., 2014. A review of approaches for evapotranspiration partitioning. Agric. For. Meteorol. 184, 56–70.

Lee, J.E., et al., 2015. Simulations of chlorophyll fluorescence incorporated into the Community Land Model version 4. Glob. Change Biol. 21 (9), 3469–3477.

Leuning, R., 1990. Modelling stomatal behaviour and photosyn-thesis of Eucalyptus grandis. Aust. J. Plant Physiol. 17, 159–175.

Leuning, R., 1995. A critical appraisal of a combined stomatal-photosynthesis model for C3 plants. Plant Cell Environ. 18, 339–355.

Li, X., et al., 2019. A simple and objective method to partition evapotranspiration into transpiration and evaporation at eddy-covariance sites. Agric. For. Meteorol. 265, 171–182.

Lombardozzi, D., Levis, S., Bonan, G., Sparks, J.P., 2012. Predicting photosynthesis and transpiration responses to ozone: decoupling modeled photosynthesis and stomatal conductance. Biogeosciences 9 (8), 3113–3130.

Lu, X.L., et al., 2018. Potential of solar-induced chlorophyll fluorescence to estimate transpiration in a temperate forest. Agric. For. Meteorol. 252, 75-+.

Maes, W.H., et al., 2020. Sun-induced fluorescence closely linked to ecosystem transpiration as evidenced by satellite data and radiative transfer models. Remote Sens. Environ. 249.

Maier, S.W., Günther, K.P., Stellmes, M., 2003. Sun-induced fluorescence: a new tool for precision farming. Dig. Imag. Spectr. Techn.: Appl. Precis. Agric. Crop Physiol. (digitalimaginga 209–222.

Manter, D.K., Kerrigan, J., 2004. A/C-i curve analysis across a range of woody plant species: influence of regression analysis parameters and mesophyll conductance. J. Exp. Bot. 55 (408), 2581–2588.

Migliavacca, M., et al., 2017. Plant functional traits and canopy structure control the relationship between photosynthetic CO2 uptake and far-red sun-induced fluorescence in a Mediterranean grassland under different nutrient availability. New Phytol. 214 (3), 1078–1091.

Miller, J.R. et al., 2005. Development of a vegetation fluorescence canopy model, Final Report, May 2005. Contract No. 16365/02/NL/FF, European Space Research and Technology Centre (ESTEC).

Miner, G.L., Bauerle, W.L., Baldocchi, D.D., 2017. Estimating the sensitivity of stomatal conductance to photosynthesis: a review. Plant Cell Environ. 40 (7), 1214–1238.

Miralles, D.G., Gentine, P., Seneviratne, S.I., Teuling, A.J., 2019. Land-atmospheric feedbacks during droughts and heatwaves: state of the science and current challenges. Ann. N. Y. Acad. Sci. 1436 (1), 19–35.

Moncrieff, J., Clement, R., Finnigan, J., Meyers, T., 2005. Averaging, detrending, and filtering of eddy covariance time series. In: Lee, X., Massman, W., Law, B. (Eds.), Handbook of Micrometeorology. Atmospheric and Oceanographic Sciences Library. Springer Netherlands, pp. 7–31.

Monteith, J.L., 1965. Evaporation and environment. Symposia of the Society for Experimental Biology 19, 205–234.

Murray, F.W., 1967. On the computation of saturation vapour pressure. J. Appl. Meteorol. 6, 203–204.

Nelson, Jacob A., et al., 2018. Coupling water and carbon fluxes to constrain estimates of transpiration: the TEA algorithm. J. Geophys. Res.: Biogeosciences 0 (0).
Nelson, J.A., et al., 2020. Ecosystem transpiration and evaporation: insights from three water flux partitioning methods across FLUXNET sites. Glob. Change Biol. 26 (12), 6916–6930.
Nobel, P.S., 2009. Physicochemical and Environmental Plant Physiology FOURTH EDITION. Elsevier Academic Press.
Pagán, B.R., Maes, W.H., Gentine, P., Martes, B., Miralles, D.G., 2019. Exploring the potential of satellite solar-induced fluorescence to constrain global transpiration estimates. Remote Sens. 11, 413.
Paul-Limoges, E., et al., 2018. Effect of environmental conditions on sun-induced fluorescence in a mixed forest and a cropland. Remote Sens. Environ. 219, 310–323.
Paul-Limoges, E., Wolf, S., Eugster, W., Hortnagl, L., Buchmann, N., 2017. Below-canopy contributions to ecosystem CO2 fluxes in a temperate mixed forest in Switzerland. Agric. For. Meteorol. 247, 582–596.
Paul-Limoges, E., et al., 2020. Partitioning water vapour fluxes with concurrent eddy covariance measurements in a mixed forest. Agric. For. Meteorol. 280, 107786.
Perez-Priego, O., et al., 2018. Partitioning eddy covariance water flux components using physiological and micrometeorological approaches. J. Geophys. Res.-Biogeosci. 123 (10), 3353–3370.
Porcar-Castell, A., et al., 2014. Linking chlorophyll a fluorescence to photosynthesis for remote sensing applications: mechanisms and challenges. J. Exp. Bot. 65 (15), 4065–4095.
Qiu, B., et al., 2018. Satellite chlorophyll fluorescence and soil moisture observations lead to advances in the predictive understanding of global terrestrial coupled carbon-water cycles. Glob. Biogeochem. Cycles 32 (3), 360–375.
Romero, P., Botia, P., Garcia, F., 2004. Effects of regulated deficit irrigation under subsurface drip irrigation conditions on water relations of mature almond trees. Plant Soil 260 (1-2), 155–168.
Rossini, M., et al., 2015. Red and far-red sun-induced chlorophyll fluorescence as a measure of plant photosynthesis. Geophys. Res. Lett. 42 (6), 1632–1639.
Ryu, Y., Berry, J.A., Baldocchi, D.D., 2019. What is global photosynthesis? History, uncertainties and opportunities. Remote Sens. Environ. 223 (15), 95–114.
Scanlon, T.M., Kustas, W.P., 2012. Partitioning evapotranspiration using an eddy covariance-based technique: improved assessment of soil moisture and land-atmosphere exchange dynamics. Vadose Zone J. 11 (3).
Schlesinger, W.H., Jasechko, S., 2014. Transpiration in the global water cycle. Agric. For. Meteorol. 189-190, 115–117.
Scott, R.L., Biederman, J.A., 2017. Partitioning evapotranspiration using long-term carbon dioxide and water vapor fluxes. Geophys. Res. Lett. 44 (13), 6833–6840.
Shan, N., et al., 2019. Modeling canopy conductance and transpiration from solar-induced chlorophyll fluorescence. Agric. For. Meteorol. 268, 189–201.
Shan, N., et al., 2021. A model for estimating transpiration from remotely sensed solar-induced chlorophyll fluorescence. Remote Sens. Environ. 252.
Short Gianotti, D.J., Rigden, A.J., Salvucci, G.D., Entekhabi, D., 2019. Satellite and station observations demonstrate water availability's effect on continental-scale evaporative and photosynthetic land surface dynamics. Water Resour. Res.
Singh, S.K., Reddy, K.R., 2011. Regulation of photosynthesis, fluorescence, stomatal conductance and water-use efficiency of cowpea (Vigna unguiculata L. Walp.) under drought. J. Photochem. Photobiol. B-Biol. 105 (1), 40–50.
Skinner, C.B., Poulsen, C.J., Mankin, J.S., 2018. Amplification of heat extremes by plant CO2 physiological forcing. Nat. Commun. 9.
Sperry, J.S., et al., 2017. Predicting stomatal responses to the environment from the optimization of photosynthetic gain and hydraulic cost. Plant Cell Environ. 40 (6), 816–830.
Steduto, P., Hsiao, T.C., Fereres, E., 2007. On the conservative behavior of biomass water productivity. Irrigation Sci. 25 (3), 189–207.
Stoy, P.C., et al., 2019. Reviews and syntheses: Turning the challenges of partitioning ecosystem evaporation and transpiration into opportunities. Biogeosciences 16 (19), 3747–3775.
Su, Z., Schmugge, T., Kustas, W.P., Massman, W.J., 2001. An evaluation of two models for estimation of the roughness height for heat transfer between the land surface and the atmosphere. J. Appl. Meteorol. 40 (11), 1933–1951.
Talsma, C.J., et al., 2018. Partitioning of evapotranspiration in remote sensing-based models. Agric. For. Meteorol. 260-261, 131–143.
Tetens, O., 1930. Über einige meteorologische Begriffe. Zeitschrift für Geophysik 6, 207–309.
Thomas, C.K., Martin, J.G., Law, B.E., Davis, K., 2013. Toward biologically meaningful net carbon exchange estimates for tall, dense canopies: Multi-level eddy covariance observations and canopy coupling regimes in a mature Douglas-fir forest in Oregon. Agric. For. Meteorol. 173, 14–27.
Trenberth, K.E., 2015. Challenges for observing and modeling the global water cycle. Editors. In: Lakshmi, V., et al. (Eds.), Remote Sensing of the Terrestrial Water Cycle. Geophysical Monograph Book Series, pp. 511–519.
Tuzet, A., Perrier, A., Leuning, R., 2003. A coupled model of stomatal conductance, photosynthesis and transpiration. Plant Cell Environ. 26 (7), 1097–1116.
van der Tol, C., Verhoef, W., Timmermans, A., Verhoef, A., Su, Z., 2009. An integrated model of soil-canopy spectral radiances, photosynthesis, fluorescence, temperature and energy balance. Biogeosciences 6, 3109–3129.
Verhoef, W., Bach, H., 2007. Coupled soil-leaf-canopy and atmosphere radiative transfer modeling to simulate hyperspectral multi-angular surface reflectance and TOA radiance data. Remote Sens. Environ. 109 (2), 166–182.
Verhoef, W., Jia, L., Xiao, Q., Su, Z., 2007. Unified optical-thermal four-stream radiative transfer theory for homogeneous vegetation canopies. IEEE Trans. Geosci. Remote Sens. 45 (6), 1808–1822.
Verrelst, J., et al., 2015. Global sensitivity analysis of the SCOPE model: what drives simulated canopy-leaving sun-induced fluorescenc? Remote Sens. Environ. 166, 8–21.
Vickers, D., Mahrt, L., 1997. Quality control and flux sampling problems for tower and aircraft data. J. Atmos. Ocean. Technol. 14 (3), 512–526.
Wang, K.C., Dickinson, R.E., 2012. A review of gobal terrestrial evapotranspiration: observation, modeling, climatology, and climatic variability. Rev. Geophys. 50.
Webb, E.K., Pearman, G.I., Leuning, R., 1980. Correction of flux measurements for density effects due to heat and water-vapor transfer. Q. J. R. Meteor. Soc. 106 (447), 85–100.
Williams, M., et al., 1996. Modelling the soil-plant-atmosphere continuum in a Quercus-Acer stand at Harvard forest: the regulation of stomatal conductance by light, nitrogen and soil/plant hydraulic properties. Plant Cell Environ. 19 (8), 911–927.
Wullschleger, S.D., 1993. Biochemical limitations to carbon assimilation in C3 plants - a retrospective analysis of the A/Ci curves from 109 species. J. Exp. Bot. 44 (262), 907–920.
Yang, P., et al., 2019. Using reflectance to explain vegetation biochemical and structural effects on sun-induced chlorophyll fluorescence. Remote Sens. Environ. 231, 110996.
Yang, P.Q., van der Tol, C., 2018. Linking canopy scattering of far-red sun-induced chlorophyll fluorescence with reflectance. Remote Sens. Environ. 209, 456–467.
Zarco-Tejada, P.J., Morales, A., Testi, L., Villalobos, F.J., 2013. Spatio-temporal patterns of chlorophyll fluorescence and physiological and structural indices acquired from hyperspectral imagery as compared with carbon fluxes measured with eddy covariance. Remote Sens. Environ. 133, 102–115.
Zhou, S., Yu, B.F., Zhang, Y., Huang, Y.F., Wang, G.Q., 2016. Partitioning evapotranspiration based on the concept of underlying water use efficiency. Water Resour. Res. 52 (2), 1160–1175.